ACS Catalysis

Research Article

pubs.acs.org/acscatalysis

Effect of the Support on the Photocatalytic Water Oxidation Activity of Cobalt Oxide Nanoclusters

Seif Yusuf and Feng Jiao*

Department of Chemical and Biomolecular Engineering, University of Delaware, Newark, Delaware 19716, United States

Supporting Information

ABSTRACT: Oxygen evolution from water driven by visible light is one of the key reactions for solar fuel production. In this paper, we investigated the effect of the support on photocatalytic water oxidation under visible light using cobalt oxide as a multielectron catalyst. A range of supported Co_3O_4 nanoclusters have been successfully synthesized via wet impregnation and bisolvent methods. Compared with the wet impregnation approach, the bisolvent method allowed us to obtain a high quality catalyst with all the Co_3O_4 nanoclusters formed inside the mesoporous support using hexane/water as the combination. The resulting catalyst consists of Co_3O_4 nanoclusters with a very small particle size (~25 nm) and narrow size distribution. Catalytic water oxidation experiments were performed in $[Ru(bpy)_3]^{2+}$-persulfate (photochemical) and Ce^{4+}/Ce^{3+} (chemical) systems, and it was found that smaller Co_3O_4 cluster sizes resulted in higher water oxidation activity. In addition, KIT-6 was found to be a better support than SBA-15, which is likely due to the fact that the 3D porous structure of KIT-6 offers more accessible pores than the 1D channels in SBA-15. To further elucidate the role of support in the photocatalytic oxygen evolution, bare Co_3O_4 nanoparticles together with two SiO_2- and γ-Al_2O_3-supported ones were investigated. Photocatalytic studies show that both supported Co_3O_4 nanoparticles exhibited significant enhancement (50−80%) in oxygen evolution activity, compared with bare Co_3O_4 nanoparticles. However, switching from the SiO_2 to γ-Al_2O_3 support does not significantly change the activities, indicating composition and surface properties of the support do not participate in rate-limiting steps in oxygen evolution. It can be concluded that the major role of catalyst supports in Co_3O_4-based water oxidation catalysts is to provide a medium to physically separate Co_3O_4 nanoclusters from aggregation, leading to superior photocatalytic activities.

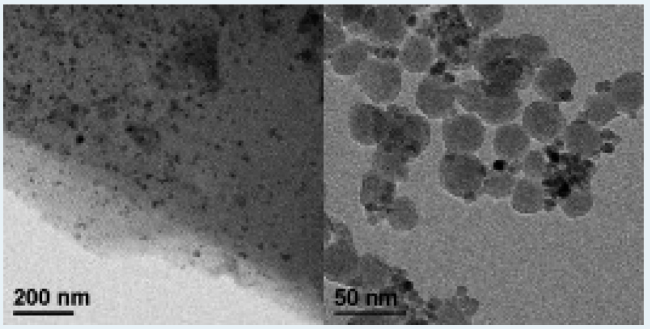

KEYWORDS: *photocatalysis, oxygen evolution, water oxidation, cobalt oxide, support effect*

INTRODUCTION

Liquid fuel demand is expected to steadily increase in the future, and fossil fuels are undesirable energy sources because they are nonrenewable. Solar energy is the largest clean and renewable energy source on the Earth, supplying 120 000 TW of radiation each year, which is more than enough to meet the growing energy demand.[1−3] To fully utilize solar energy as a major energy source, solar energy must be harvested and converted into an alternative form that can be easily stored and transported (e.g., CH_3OH). One approach is to produce solar fuels from abundant sources via photocatalysis, which is also referred to as artificial photosynthesis.[3−7] For example, many research efforts have been made in visible-light-driven water-splitting using semiconductors to produce solar hydrogen and photocatalytic reduction of carbon dioxide to methanol.[8−12]

Oxygen evolution from water is the key reaction for solar fuel production because water oxidation under sunlight is known to be the only cheap and abundant source that is able to supply protons and electrons in a terawatt scale.[13−23] In nature, plants effectively catalyze water oxidation using visible light through the combination of chrolophyll complexes (to absorb light and separate holes and electrons) and a $CaMn_4O_4$ complex (to act as the site of water oxidation). It is crucial to have two separated components in the system, one for light capture (e.g., sensitizer) and the other for a multielectron catalytic reaction, to maximize both sunlight utilization and catalytic activity. In artificial photosynthesis, a $[Ru(bpy)_3]^{2+}$-$Na_2S_2O_8$ system has been established, which allows us to decouple the catalytic reaction from the light capture process.[15,16] Using $[Ru(bpy)_3]^{2+}$ (bpy = 2,2′-bipyridine) as the sensitizer and sodium persulfate as the sacrificial electron acceptor, Mallouk and his co-workers demonstrated that IrO_2 colloid is a remarkable catalyst for water oxidation with a TOF of 40 s^{-1} per surface Ir atom under an aqueous environment (pH 5.7, 25 °C).[16] However, iridium is one of the least abundant elements on the Earth, which prevents it from practical large-scale applications. As alternatives, first-row transition metal oxides, e.g. cobalt and manganese oxides, have attracted much attention as potential

Received: September 4, 2012
Revised: November 2, 2012
Published: November 9, 2012

   dx.doi.org/10.1021/cs300581k | ACS Catal. 2012, 2, 2753−2760

water oxidation catalysts because they are abundant and cheap.[5,24−44] Harrison, Pickering, Thomas and Christensen performed a detailed study on micrometer-sized cobalt and manganese oxides,[15] and they showed that both Co_3O_4 and Mn_2O_3 are active as oxygen evolution catalysts driven by visible light.

We recently reported the first example of cobalt oxide nanoclusters in a mesoporous silica support as efficient and robust catalysts.[45] Co_3O_4 nanoclusters embedded inside a mesoporous silica SBA-15 support with two different loading levels (i.e., 4 and 8 wt %) were obtained via a wet impregnation method. The larger Co_3O_4 clusters (8 wt % sample) exhibit a somehow lower TOF of 0.5 s^{-1} nm^{-2} compared with the TOF (1 s^{-1} nm^{-2}) of 35 nm diameter clusters (4 wt % sample). One interesting observation by comparing the TOFs of the nanostructured Co_3O_4 clusters in mesoporous silica SBA-15 with those of micrometer-sized bare Co_3O_4 particles (no silica support) is that the O_2 yield per second is 1550 times larger for 35 nm clusters in SBA-15 than for micrometer sized Co_3O_4 particles if normalized to the same weight. Even after normalizing the TOFs using the number of surface atoms (96 times difference), the activity for Co_3O_4 nanoclusters supported in SBA-15 is still 16 times higher that of bare Co_3O_4 micrometer particles. Our speculation of the origin of additional 16 times difference is that mesoporous silica support may promote the activities of surface cobalt atoms, possibly by suppressing surface restructuring. The silica support may also assist deprotonation during photocatalysis and, thus, enhance the proton diffusion and improves the kinetics of the catalytic sites.

In this paper, to further elucidate the role of support in photocatalytic water oxidation, we investigated the photocatalytic activity of cobalt oxide nanoparticles with different SiO_2 or γ-Al_2O_3 supports. Two mesoporous silica supports, SBA-15 and KIT-6, were synthesized and loaded with Co_3O_4 nanoclusters inside their channels using bisolvent and wet-impregnation methods. The resulting catalysts were systematically investigated as multielectron oxygen evolution catalysts in a well-established $[Ru(bpy)_3]^{2+}$-$Na_2S_2O_8$ system to explore how the supports affect the photocatalytic activities.

EXPERIMENTAL METHODS

Synthesis of Mesoporous Silica KIT-6. The synthesis of mesoporous silica KIT-6 was previously reported by Kleitz and his co-workers.[46] A 20 g portion of triblock copolymer P123 (Sigma Aldrich, M_n ~5800) was dissolved in a mixture of 750 mL of deionized H_2O and 34 mL of HCl (Sigma Aldrich, 37 wt %), then 20 g of 1-butanol (Sigma Aldrich, 99.8%) was added, and the mixture was stirred at 34 °C for one hour. After that, 43 g of tetraethyl orthosilicate (TEOS, Sigma Aldrich, 98%) was added, and the mixture was stirred for 24 h at 34 °C. The resulting mixture was transferred into polypropylene bottles, sealed, and subjected to hydrothermal treatment at 100 °C for another 24 h. After hydrothermal treatment, the mixture was filtered and treated with a mixture composed of 30 mL of HCl and 300 mL of ethanol and washed with DI water. The resulting powder was dried and calcinated at 550 °C for 3 h in air at a ramp rate of 2 °C/min to remove the polymer template.

Synthesis of Mesoporous Silica SBA-15. The synthesis of mesoporous silica SBA-15 was previously reported by Zhao and his co-workers.[47] A 20 g portion of triblock copolymer P123 (Sigma Aldrich, M_n ~5800) was added to a mixture of 750 mL of deionized H_2O and 40 mL of 37 wt % HCl. Once fully dissolved, 44 g of TEOS was added, and the mixture was stirred at 40 °C for 24 h. The mixture was then transferred into polypropylene bottles, sealed, and maintained at 100 °C for another 24 h. After that, the mixture was filtered, washed with DI water, dried, and calcinated at 500 °C for 3 h with a ramp rate of 2 °C/min.

Synthesis of Mesoporous Silica-Supported Co_3O_4 catalysts. The cobalt content in the final catalyst is set to 4% by weight as an optimal loading according to our previous findings in Co_3O_4-loaded SBA-15 catalysts.[45] Two different methods were used to load cobalt onto the mesoporous silica supports: wet impregnation and bisolvent[48−50] For wet impregnation, 0.208 g of $Co(NO_3)_2{\cdot}6H_2O$ (7.17×10^{-4} mol Co, Sigma Aldrich, 98%) was dissolved in 2 mL of ethanol. The solution was added to 1 g of mesoporous silica (SBA-15 or KIT-6) dropwise, followed by drying at 60 °C. For the bisolvent method, 1 g of mesoporous silica support was dispersed in 20 mL of either hexane (Alfa Aesar, environmental grade) or pentane (Sigma Aldrich, 98%). One milliliter of an aqueous solution of $Co(NO_3)_2{\cdot}6H_2O$ (containing 7.17×10^{-4} mol Co) was added dropwise to the silica dispersion under stirring. After stirring for another 1 h, the mixture was filtered and dried at 60 °C. To convert the cobalt precursor to Co_3O_4, all dried samples were heated in air to 700 °C at a ramp rate of 2 °C/min. Once 700 °C was reached, the samples were cooled naturally to room temperature.

Synthesis of Nanoparticle-Supported Co_3O_4 Catalysts. Two different nanoparticles, SiO_2 and Al_2O_3, were used as support to study the influence of support composition on photocatalytic oxygen evolution from water. Both nanoparticle supports were obtained from Sigma Aldrich (SiO_2: LUDOX TM-40, 420786 and Al_2O_3: nanopowder, 718475). SiO_2 and Al_2O_3 nanoparticles have average particle diameters of 25 ± 3 and 13 nm, respectively. The Co_3O_4 nanoparticles were synthesized according to a previously published procedure. A 0.50 g portion of $Co(CH_3COO)_2{\cdot}4H_2O$ was dissolved in 2.0 mL of DI water and 23.0 mL of ethanol in a 40 mL Teflon liner, and then 2.5 mL of 28% ammonia was added to the cobalt solution, and the mixture was stirred for 10 min. The liner was inserted into an autoclave and heated at 150 °C for 3 h. After heat treatment, the autoclave was cooled to room temperature, and the product was washed with DI water through centrifugation−redispersion. The final product was then dried at 60 °C overnight. In a typical cobalt loading, 0.02 g of as-made Co_3O_4 nanoparticles was dispersed in 15 mL of methanol, and the resulting solution was added to either 0.85 g of LUDOX TM-40 solution (40% SiO_2) or 0.34 g of Al_2O_3 nanoparticles. The mixture was stirred in a fume hood overnight until a dried powder was obtained. Finally, the powders were heated in air at 200 °C for 1 h to obtain the product (~4 wt % Co loading).

Structural Characterization. All powder X-ray diffraction (PXRD) measurements were performed with a Rigaku Ultima IV diffractometer using Cu Kα radiation. Transmission electron microscopy (TEM) was performed with a JEOL JEM-2010F field-emission transmission electron microscope using an accelerating voltage of 200 kV. Surface area, pore size and pore volume measurements were performed using an isothermal nitrogen adsorption/desorption instrument. Inductively coupled plasma optical emission spectrometry (ICP-OES) analysis was carried out in the Soil Lab at the University of Delaware.

Photocatalytic Oxygen Evolution from Water. Photochemical water oxidation experiments were conducted in a 100 mL reactor containing 40 mL of aqueous buffer (Na_2SiF_6–$NaHCO_3$) at pH 5.8, 390 mg of Na_2SO_4, 130 mg of $Na_2S_2O_8$, and 75 mg of the as-synthesized catalyst. The amount of $[Ru(bpy)_3]Cl_2·6H_2O$ sensitizer added to the reactor was varied in the range of 20–100 mg to determine the optimal ratio between catalyst and sensitizer. The light source was a 300 W Xe research lamp (UV fused silica, 1.3 in. collimated, F/1, 1.5 in.) with 400 nm cutoff filter. The resulting O_2 molecules in the head space were quantitatively analyzed by a Shimadzu gas chromatography system (Shimadzu GC-2014) equipped with a PDHID detector. All the experiments were conducted at room temperature (~25 °C). A baseline was recorded for each experiment to confirm no leakage in the system.

A control experiment was done with a reduced amount of catalyst in the reactor. This test was to determine if the overall cycle is limited by the catalytic oxygen evolution step on the catalyst surface. To study the intrinsic catalytic activity of the proposed catalysts, the oxygen yield must be limited by the catalytic reaction on the Co_3O_4 surface. We reduced the amount of catalyst from 75 to 25 mg and observed the change in the amount of O_2 generated.

Chemical Oxygen Evolution from Water. Chemical water oxidation experiments were performed using Ce^{4+} as the sacrificial electron acceptor to chemically oxidize water to the oxygen molecule. The oxygen evolution was monitored in a Clark electrode system, and the TOFs were calculated using the total oxygen yield after 120 s of reaction. In a typical reaction, 1 mL of DI water was placed in the Clark electrode system, followed by the addition of 2.5 mg of catalyst. The solution was bubbled with nitrogen for about 10 min to remove dissolved oxygen. After bubbling, the system was maintained as is for another 10 min to record a baseline before 0.2 mL of Ce^{4+} aqueous solution (2.4 M) was injected to initiate the chemical water oxidation.

RESULTS AND DISCUSSION

In our previous study, we have reported the preparation of Co_3O_4 nanoclusters supported in mesoporous silica SBA-15 through a wet impregnation method. SBA-15 consists of one-dimensional (1D) channels with a hexagonal symmetry.[47] The average pore diameter of the main channels is ~7–8 nm, and the main channels are interconnected via micropores (1–2 nm in diameter). The cobalt oxide cluster formed inside the channels of SBA-15 replicated its pore structure, resulting in a bundle-like morphology. Here, we chose mesoporous silica (KIT-6) as the catalyst support, which has bicontinuous three-dimensional (3D) pores throughout the whole particle.[46] With such 3D pores, KIT-6 as a catalyst support offers better accessibility for reagents to reach the surface of Co_3O_4 clusters (catalytic site for water evolution).

A KIT-6/Co_3O_4 catalyst was first synthesized using a wet impregnation method (denoted as KIT-6/Co_3O_4-WI). To confirm the success of Co_3O_4 cluster formation inside the mesopores of KIT-6, TEM analysis was performed. A typical image of KIT-6/Co_3O_4-WI is shown in Figure 1a. The dark dots in the image represent the cobalt oxide particles. Clearly, cobalt oxide nanoclusters were successfully loaded into the channels of KIT-6, and no large particle of cobalt oxide was formed outside the channels. It can also be seen from Figure 1a that the Co_3O_4 cluster sizes in KIT-6/Co_3O_4-WI have a wide distribution, from 30 to 200 nm.

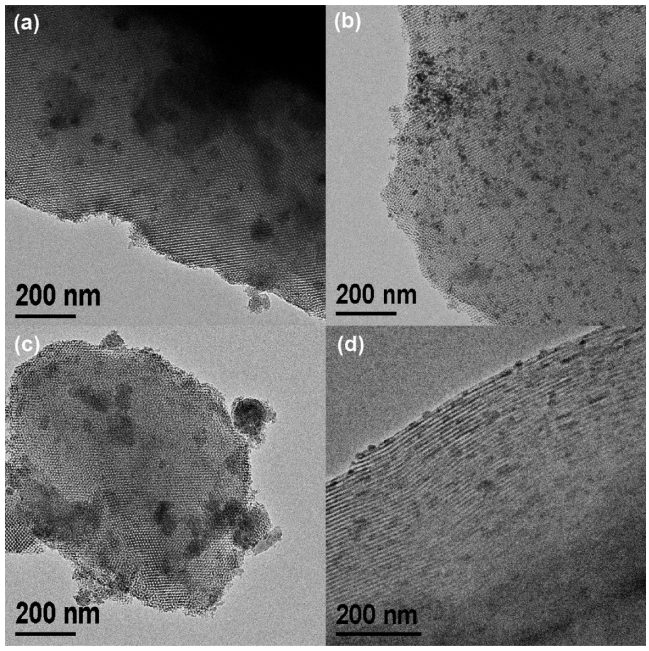

Figure 1. TEM images for (a) KIT-6/Co_3O_4-WI, (b) KIT-6/Co_3O_4-HEX, (c) KIT-6/Co_3O_4-PEN, and (d) SBA-15/Co_3O_4-HEX.

To prepare smaller clusters with a narrow size distribution, the bisolvent method, which has been reported to be an effective approach to load a metal precursor into the hydrophilic silica channels was employed,.[49,50] Here, we chose hexane and pentane as nonpolar solvents, and the resulting catalysts are denoted as KIT-6/Co_3O_4-HEX and KIT-6/Co_3O_4-PEN, respectively. The morphologies of as-prepared KIT-6/Co_3O_4-HEX and KIT-6/Co_3O_4-PEN were examined by TEM. It can be seen from the TEM images (Figure 1b and c) that KIT-6/Co_3O_4-HEX contains very small Co_3O_4 nanoclusters (below 25 nm) with a narrow size distribution, whereas the clusters in KIT-6/Co_3O_4-PEN are much bigger (~50–200 nm), and Co_3O_4 particles formed outside the pores were also observed. The TEM results confirm that hexane is a better choice than pentane for small cluster formation in the bisolvent method, although in a previous report, the authors claimed that pentane is more effective over hexane.[50]

Following this finding, we synthesized a mesoporous silica SBA-15 version of catalyst (SBA-15/Co_3O_4-HEX) through the bisolvent method using hexane as the nonpolar solvent to make comparison with KIT-6/Co_3O_4-HEX. Because KIT-6 has a pore dimension similar to SBA-15 (~7–8 nm) and its main channels are interconnected via small pores (1–2 nm), as well, a detailed comparison between SBA-15/Co_3O_4-HEX and KIT-6/Co_3O_4-HEX allows us to investigate how the pore dimension of the silica support (i.e., 1D vs 3D) affects the activity of Co_3O_4 clusters. A typical TEM image of SBA-15/Co_3O_4-HEX is shown in Figure 1d, and well-dispersed small clusters can be clearly observed. On the basis of TEM analysis, the statistical sizes of Co_3O_4 clusters are summarized in the left column of Table 1.

Via TEM (Figure 1) as well as low angle powder X-ray diffraction (PXRD) (Figure 2a) analysis, silica supports are confirmed to maintain highly ordered mesostructures in all the catalysts. For the samples using KIT-6 as the support, two low-angle diffraction peaks at 0.97° and 1.12° corresponding to [211] and [200] diffractions plus one broad peak at ~1.7° were

dx.doi.org/10.1021/cs300581k | ACS Catal. 2012, 2, 2753–2760

Table 1. Average Cluster Sizes Estimated from TEM Data and Crystallinity Sizes Calculated from the Scherrer Formula for All Catalysts

catalyst	av cluster size (nm)	crystallinity size (nm)
KIT-6/Co_3O_4-WI	51	10
KIT-6/Co_3O_4-HEX	25	8
KIT-6/Co_3O_4-PEN	142	15
SBA-15/Co_3O_4-HEX	30	11

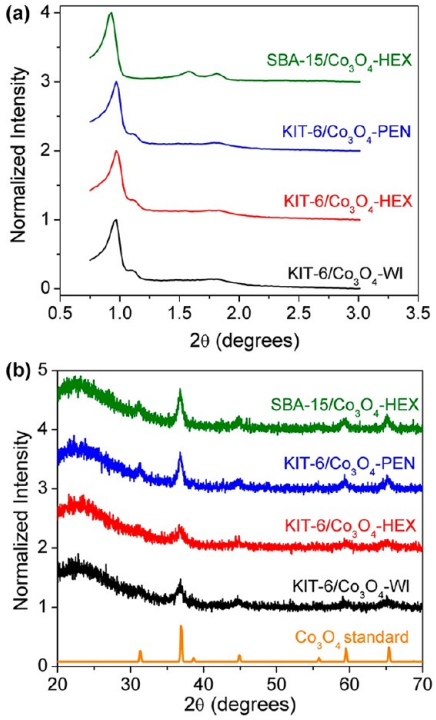

Figure 2. (a) Low-angle and (b) high-angle PXRD patterns for KIT-6/Co_3O_4-WI, KIT-6/Co_3O_4-HEX, KIT-6/Co_3O_4-PEN, and SBA-15/Co_3O_4-HEX. A standard PXRD pattern for bulk Co_3O_4 is also shown in part b for comparison.

observed, indicating that well-ordered mesoporous structure of KIT-6 was preserved throughout the whole sample preparation procedure. For SBA-15/Co_3O_4-HEX, the PXRD pattern shows a sharp peak at 0.92° and two well-defined peaks at 1.58° and 1.82°, confirming the presence of an ordered mesostructure with a hexagonal symmetry. The low-angle PXRD results are in good agreement with the TEM data. Nitrogen adsorption–desorption measurements were also performed, and the results (Table 2) confirmed that the average pore sizes for KIT-6- and SBA-15-supported catalysts are 5.4 and 6.0 nm, respectively, which are consistent with literature values.[44,45] Note that a large pore volume and BET surface area have been maintained after

Table 2. Structural Information for Mesoporous Silica Supported Cobalt Catalysts Obtained from Nitrogen Adsorption Experiments

sample	pore size (nm)	pore volume (cm^3/g)	BET (m^2/g)
KIT-6/Co_3O_4-HEX	5.4	0.85	603.7
KIT-6/Co_3O_4-WI	5.4	0.91	625.0
KIT-6/Co_3O_4-PEN	5.4	0.91	656.3
SBA-15/Co_3O_4-HEX	6.0	0.84	554.4

cobalt oxide loading, indicating that Co_3O_4 nanoclusters did not block the mesopores in the silica support.

Turning to the atomic level structure of the as-made catalysts, high-angle PXRD analysis was used as a standard technique to determine the crystal structures of cobalt oxide particles formed inside the silica supports. High-angle PXRD patterns for all the as-made samples are shown in Figure 2b, and several diffraction peaks that closely match the standard PXRD pattern for bulk Co_3O_4 spinel can be clearly observed. These results confirmed that cobalt oxide nanoclusters in all the samples have an identical Co_3O_4 spinel structure, regardless of the geometry of supports and synthetic methods. A broad peak at 22–23° is observed, and it may result from the amorphous silica support. The diffraction peaks in Figure 2b are significantly broadened, suggesting the nanocrystalline nature of Co_3O_4 spinel in these samples. The Scherrer formula was used to estimate the crystallinity size of Co_3O_4, and the results are listed in Table 1. Because the diffraction peaks for all the samples are poorly defined, the calculated crystallinity domain size for each sample in Table 1 is only a rough estimate. For KIT-6/Co_3O_4-WI, KIT-6/Co_3O_4-HEX, and SBA-15/Co_3O_4-HEX, the estimated crystal domain sizes closely match the pore dimension of mesoporous silica supports (7–8 nm), suggesting that the Co_3O_4 nanoclusters are well confined in the channels of mesoporous supports. However, KIT-6/Co_3O_4-PEN has an estimated crystal domain size of 15 nm, larger than the pore dimension. It is likely due to some of the large Co_3O_4 particles formed outside the mesopores (Figure 1c).

The as-synthesized mesoporous silica-supported cobalt oxide catalysts were also examined by FTIR and UV–vis analysis. The FTIR results in Supporting Information Figure S1 show two bands at ~660 and 570 cm^{-1} associated with Co–O bond stretching. This observation is consistent with a previous report for nanoparticle Co_3O_4.[51] Turning to the UV–vis spectra (Supporting Information Figure S2), all the catalysts show two very broad and weak peaks at approximately 420 and 720 nm, resulting from Co_3O_4 nanoclusters.[52] Both FTIR and UV–vis results confirmed the successful preparation of Co_3O_4 nanoclusters in the mesoporous silica support, in good agreement with PXRD data.

Photocatalytic water oxidation experiments were carried out using the $[Ru(bpy)_3]^{2+}$–$S_2O_8^{2-}$ system in an aqueous buffer (Na_2SiF_6–$NaHCO_3$) at pH 5.8. $[Ru(bpy)_3]^{2+}$ is the sensitizer, which absorbs visible light and generates electron–hole pairs. The generated electrons are taken up by the sacrificial electron acceptor $S_2O_8^{2-}$, causing $[Ru(bpy)_3]^{2+}$ to be oxidized to $[Ru(bpy)_3]^{3+}$ and $S_2O_8^{2-}$ to be reduced to one SO_4^{2-} and one SO_4^{-}* radical. The SO_4^{-}* radical can subsequently oxidize another molecule of $[Ru(bpy)_3]^{2+}$ to $[Ru(bpy)_3]^{3+}$. $[Ru(bpy)_3]^{3+}$ molecules donate the holes to the oxygen evolution catalyst and return to the $[Ru(bpy)_3]^{2+}$ state.[15] Such a cycle, as shown in Figure 3, has to be repeated twice to produce one molecule of O_2. Control tests were performed to confirm that when any one of the three main components of this system (sensitizer, light source, and catalyst) was missing, no O_2 evolution could be observed.

A series of experiments was performed to determine the optimal sensitizer concentration by fixing the catalyst weight at 75 mg and changing the concentration of $[Ru(bpy)_3]^{2+}$ from 6.7×10^{-4} to 3.3×10^{-3} mol·L^{-1}. KIT-6/Co_3O_4-HEX was used as a standard catalyst in this study because of its small particle size and narrow size distribution. After 30 min of visible light radiation (300 W, >400 nm), oxygen concentration in the head

dx.doi.org/10.1021/cs300581k | ACS Catal. 2012, 2, 2753–2760

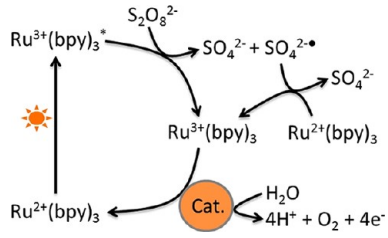

Figure 3. A schematic diagram of visible-light-driven oxygen evolution in the $[Ru(bpy)_3]^{2+}$–$S_2O_8^{2-}$ system.

space was measured using GC. The turnover frequencies (TOFs) per Co atom were calculated from the oxygen yield; the results are plotted in Figure 4. As the concentration of

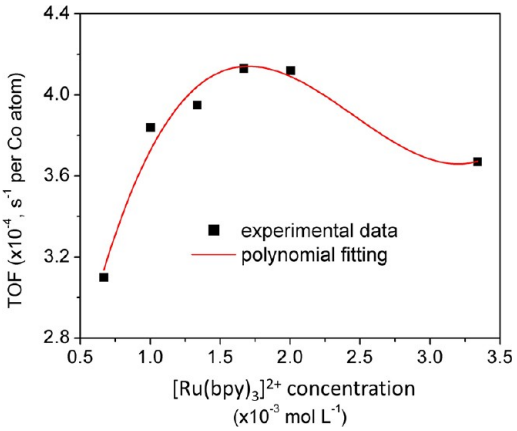

Figure 4. Sensitizer–TOF relationship using KIT-6/Co_3O_4-HEX as the catalyst.

$[Ru(bpy)_3]^{2+}$ increased, the TOF increased to reach a peak and then decreased. The decrease in the TOF at high sensitizer concentration is caused by a "shielding" effect, which was also observed in the IrO_2 system.[16] When the concentration of $[Ru(bpy)_3]^{2+}$ is too high, a significant amount of incident photons will be absorbed by the free $[Ru(bpy)_3]^{2+}$ molecules in the solution, and therefore, fewer photons can be accessed for the sensitizer molecules on the catalyst surface, resulting in a low oxygen evolution rate. An optimal $[Ru(bpy)_3]^{2+}$ concentration of $\sim 1.7 \times 10^{-3}$ mol·L^{-1} is estimated from a polynomial fitting, and all the remaining oxygen evolution experiments were performed at the optimal concentration to achieve a maximum of oxygen evolution rate.

To investigate the intrinsic activity of the catalyst, the whole water oxidation cycle (Figure 3) has to be limited by the rate of oxygen molecule formation on the catalyst surface. To confirm that, we varied the amount of sodium persulfate in the system, and the same initial oxygen evolution rate was observed, confirming that the electron transfer from sensitizer to persulfate (sacrificial electron acceptor) is not the rate-limiting step. After that, another control experiment at an identical condition, except using only half the amount of the catalyst, was performed. The oxygen yield was reduced by 50% with half the amount of the catalyst, confirming that catalytic reaction on the surface of the catalyst is the rate-limiting step in our system.

The oxygen yields for KIT-6/Co_3O_4-WI, KIT-6/Co_3O_4-PEN, and SBA-15/Co_3O_4-HEX that were measured using 75 mg of catalyst and 50 mg of $[Ru(bpy)_3]Cl_2 \cdot 6H_2O$ (i.e., $[Ru(bpy)_3]^{2+}$, 1.7×10^{-3} mol·L^{-1}) are listed in Table 3. We repeated the photochemical reaction at least three times to ensure good reproducibility (within ±5% difference). The accurate cobalt loading in each sample was confirmed by ICP-OES analysis and is in agreement with the estimated value (~4 wt % Co). In 30 min of visible light radiation, the KIT-6/Co_3O_4-HEX exhibited the highest rate of O_2 evolution from water (70.5 μmol·h^{-1}), and the KIT-6/Co_3O_4-PEN catalyst showed a much lower rate (36.7 μmol·h^{-1}). We attribute such a difference in oxygen evolution activities to their cluster sizes in the KIT-6 support. From the TEM and high-angle PXRD data, it is clear that KIT-6/Co_3O_4-PEN has a much larger cluster size and crystallinity domain size, when compared with KIT-6/Co_3O_4-HEX.

The difference in cluster sizes results in a different number of surface catalytic sites that are available for photocatalytic water oxidation in both samples. The sample obtained from the wet impregnation method has a medium cluster size (70 nm) and exhibits a TOF of 3.27×10^{-4} s^{-1} per Co atom, higher than that of KIT-6/Co_3O_4-PEN but lower than that of KIT-6/Co_3O_4-HEX. This observed TOF is consistent with our expectation based on structural characterization results (Table 1). Turning to SBA-15/Co_3O_4-HEX, it exhibits a TOF of 3.38×10^{-4} s^{-1} per Co atom, which is lower than that of KIT-6/Co_3O_4-HEX but close to that of KIT-6/Co_3O_4-WI. Because SBA-15/Co_3O_4-HEX has a particle size similar to that of KIT-6/Co_3O_4-HEX, it is concluded that such an increase in the TOF for KIT-6/Co_3O_4-HEX is mainly due to the 3D porous support (KIT-6), which offers better accessibility than 1D channels of SBA-15. A detailed comparison among all the transition metal oxide catalysts is shown in Table 4. It is evident that the water oxidation activities per cobalt atom reported here are of the same order of magnitude compared with other previous reports.

In addition to the $[Ru(bpy)_3]^{2+}$–$S_2O_8^{2-}$ system, we also investigated water oxidation activities of supported catalysts using Ce^{4+} as an oxidant to chemically oxidize water to oxygen. Ce^{4+} has a standard chemical potential E^0 = 1.7 V vs NHE in acidic conditions, which is enough to oxidize water to oxygen in a chemical manner. Here, we utilize a Ce^{4+}/Ce^{3+} system as an

Table 3. TOFs for All Supported Catalysts

		O_2 yield (μmol·h^{-1})		TOF (s^{-1} per Co atom) × 10^4	
catalyst	cobalt content (wt %)	photochemical[a]	chemical[b]	photochemical[a]	chemical[b]
KIT-6/Co_3O_4-WI	3.8	57.1 ± 0.3	2.0 ± 0.1	3.27 ± 0.02	3.4 ± 0.1
KIT-6/Co_3O_4-HEX	3.7	70.5 ± 1.7	3.0 ± 0.2	4.05 ± 0.10	5.3 ± 0.4
KIT-6/Co_3O_4-PEN	3.8	36.7 ± 1.1	2.0 ± 0.2	2.12 ± 0.06	3.4 ± 0.3
SBA-15/Co_3O_4-HEX	4.0	62.8 ± 2.8	2.1 ± 0.1	3.38 ± 0.15	3.4 ± 0.1

[a] $[Ru(bpy)_3]^{2+}$–$S_2O_8^{2-}$ system; 75 mg of catalyst and 50 mg of $[Ru(bpy)_3]^{2+}$ were used; oxygen measured by GC. [b] Ce^{4+}/Ce^{3+} system; oxygen measured by Clarke electrode.

dx.doi.org/10.1021/cs300581k | ACS Catal. 2012, 2, 2753–2760

Table 4. Water Oxidation Activities for Various Cobalt and Manganese Oxides

catalyst	TOF (s^{-1} per Co/Mn atom)[a]	overpotential (mV)	pH	ref
$Li_2Co_2O_4$	1.0×10^{-3}	325	5.8	53
Co_3O_4	1.4×10^{-4}	325	5	15
$NiCo_2O_4$	7.9×10^{-5}	325	5	15
Co−P film	7×10^{-4}	410	7.0	18
SBA-15/Co_3O_4	6.4×10^{-4}	325	5.8	45
$CaMnO_4 \cdot H_2O$	1.5×10^{-4}	325	4.0	26
KIT-6/Mn_xO_y	2.8×10^{-4}	325	5.8	25
$LaCoO_3$	6.5×10^{-4}	325	7	54

[a]Lower limit by assuming all cobalt atoms are active in the catalyst.

alternative approach to study water oxidation activities in mesoporous silica-supported cobalt catalysts. The results for all the mesoporous silica-supported cobalt catalysts are shown in Table 3. It is evident that KIT-6/Co_3O_4-HEX is still the best catalyst, whereas the other three catalysts exhibited a similar activity. Such differences in oxygen evolution activities could be a result of the size difference between $[Ru(bpy)_3]^{2+}$ and Ce^{4+} cations. Because the Ce^{4+} cation has a much smaller size, it might be able to access extra surface sites that $[Ru(bpy)_3]^{2+}$ cannot reach.

Superior stability of Co_3O_4 nanoclusters embedded in mesoporous silica support has been demonstrated in our previous work.[45] Here, we also investigated the preservation of the ordered mesoporous structure of the support and the crystal structure of Co_3O_4 clusters before and after the photocatalytic reaction. The low-angle PXRD patterns for KIT-6/Co_3O_4-HEX before and after 1 h of photolysis are displayed in Figure 5a, which clearly demonstrates that the ordered mesoporous structure of KIT-6/Co_3O_4-HEX was preserved after photocatalytic water oxidation. The high-angle PXRD patterns (Figure 5b) confirm that the cobalt oxide clusters in KIT-6/Co_3O_4-HEX after reaction maintained their Co_3O_4 spinel structure.

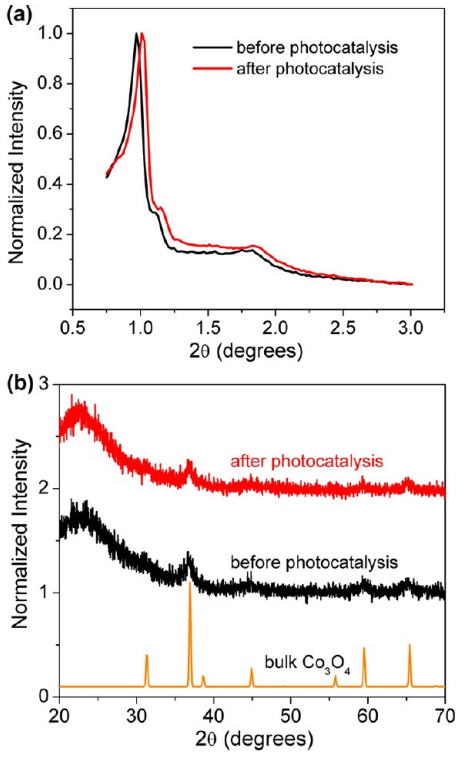

Figure 5. Low- and high-angle PXRD patterns for KIT-6/Co_3O_4-HEX before and after photocatalysis.

One question that has not yet been answered is the role of silica in the photocatalytic oxygen evolution from water. As we noticed from previous work, there is still a factor of 16 times difference in oxygen evolution activity, which cannot be explained simply by the surface area of Co_3O_4 nanoclusters.[45] Our speculation is that the curved mesoporous silica channels may help suppress surface active site restructuring and assisting in the depronation process. To test this hypothesis, well-defined Co_3O_4 nanoparticles (diameter ~ 6 nm) were used as model catalysts and loaded onto two different nanoparticulate supports, SiO_2 and Al_2O_3 (denoted as nano-SiO_2/Co_3O_4 and nano-Al_2O_3/Co_3O_4, respectively). The detailed procedure for sample preparation is described in the Experimental section.

Detailed structural characterizations were performed for all the as-prepared samples before photocatalytic studies. The as-prepared Co_3O_4 nanoparticles show clear diffraction peaks (Figure 6), closely matching the standard Co_3O_4 with a spinel

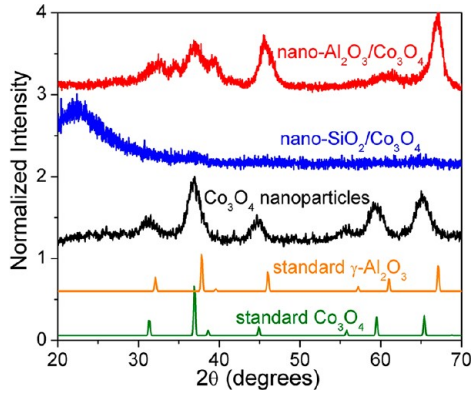

Figure 6. PXRD patterns for as-prepared Co_3O_4 nanoparticles, nano-SiO_2/Co_3O_4, and nano-Al_2O_3/Co_3O_4.

structure. After loading Co_3O_4 nanoparticles (~4 wt % in final product) onto SiO_2 and γ-Al_2O_3 supports, only very weak and broad diffraction peaks for the Co_3O_4 spinel phase could be observed (Figure 6) due to the low concentration of Co_3O_4 in the final catalysts. Typical TEM images for the three catalysts are shown in Figure 7. It is evident that as-prepared Co_3O_4 nanoparticles have a spherical shape and a particle size of 6 ± 2 nm with a narrow distribution (Figure 7a). The lattice fringes of Co_3O_4 nanoparticles can be clearly observed in the HRTEM image (Figure 7b), and the observed distance between two lattice fringes is ~0.20 nm, which matches the distance between [400] planes in the Co_3O_4 spinel structure. For the nano-SiO_2/Co_3O_4, it is evident that the Co_3O_4 nanoparticles are well dispersed in the SiO_2 nanoparticles (Figure 7c), and in the HRTEM image (Figure 7d), we clearly observed the lattice fringes with a distance of 0.28 nm that matches the d space for the [220] planes of Co_3O_4 spinel. However, for the nano-Al_2O_3/Co_3O_4 catalyst (Figures 7e, f), it is difficult to distinguish the Co_3O_4 particles from the Al_2O_3 particles, since both materials are crystalline. We did not observe any large particles in either sample, suggesting that most of the nanoparticles are well dispersed throughout the catalysts.

dx.doi.org/10.1021/cs300581k | ACS Catal. 2012, 2, 2753−2760

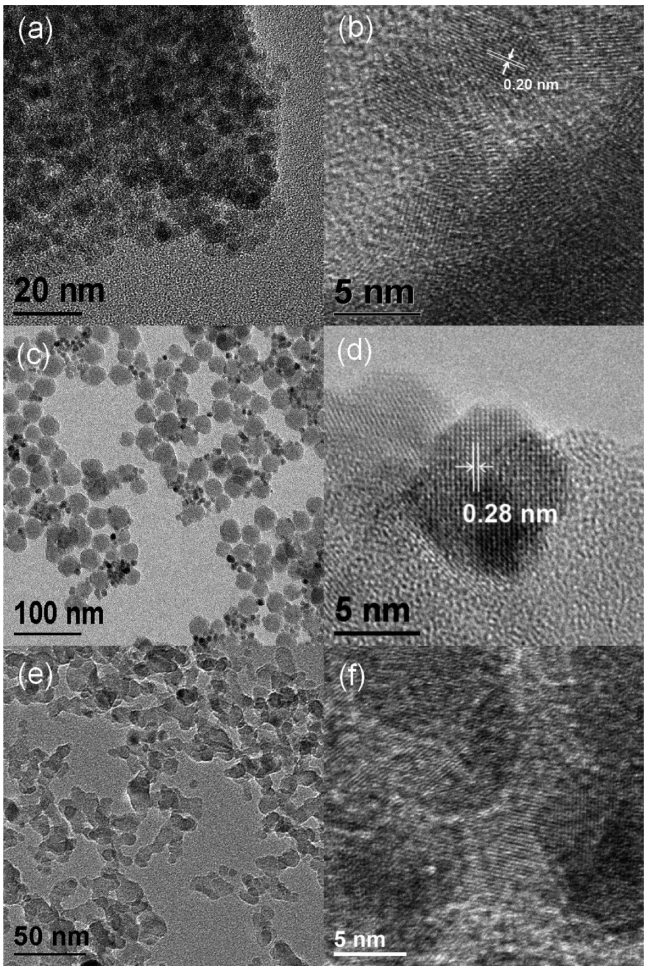

Figure 7. TEM and HRTEM images for (a, b) as-made Co_3O_4 nanoparticles, (c, d) nano-SiO_2/Co_3O_4, and (e, f) nano-Al_2O_3/Co_3O_4.

Photocatalytic water oxidation experiments were performed using two catalysts with a nanoparticulate support and the same amount of Co loading. The other conditions were fixed at the same amount as those used in previous studies. The results are summarized in Table 4. It can be seen that nano-Al_2O_3/Co_3O_4 exhibited a 26% higher oxygen evolution activity than that of nano-SiO_2/Co_3O_4. The reason why nano-Al_2O_3/Co_3O_4 is more active is likely the fact that the surface area of Al_2O_3 (~140 m^2 g^{-1}) is larger than that of SiO_2 (~100 m^2 g^{-1}), resulting in a better physical separation of Co_3O_4 nanoparticles. Considering that a 26% difference in activity is not significant, it is less likely that either a SiO_2 or Al_2O_3 support is directly involved in the oxygen molecule formation on the cobalt oxide surface. Therefore, we conclude that the key role of the support in the photocatalytic reaction is to physically separate catalytic particles from aggregation. Such a physical separation is essential to avoid active site aggregation, as was shown in the control experiment that pure Co_3O_4 nanoparticles exhibited a much lower activity (TOF, 2.5×10^{-4} s^{-1} per Co atom) as an oxygen evolution catalyst than did supported catalysts under identical conditions (Table 5).

CONCLUSION

We have successfully synthesized a range of Co_3O_4 nanoclusters supported by various substances, including mesoporous silica KIT-6, mesoporous silica SBA-15, SiO_2 nanoparticles, and γ-Al_2O_3 nanoparticles. A bisolvent method was used to obtain a high-quality catalyst with all the Co_3O_4 nanoclusters formed inside the mesoporous support through a hydrophilic–hydrophobic interaction. Hexane has been proven to be a better nonpolar solvent in the bisolvent approach than pentane, and the resulting catalyst consists of Co_3O_4 nanoclusters with a small particle size and narrow size distribution. Photocatalytic water oxidation activities of as-synthesized catalysts were investigated using the $[Ru(bpy)_3]^{2+}$-persulfate system. The results confirmed that smaller Co_3O_4 cluster size and higher water oxidation activity. Compared with SBA-15, KIT-6 was found to be a better support, which is likely due to its 3D porous structure offering a more accessible system. To elucidate the role of the support in the photocatalytic oxygen evolution, we compared bare Co_3O_4 nanoparticles with supported ones. Although both SiO_2 and γ-Al_2O_3 supported catalysts exhibited higher activities than bare nanoparticles, switching from SiO_2 to γ-Al_2O_3 did not influence their activity in a significant way. The results indicate that the composition and surface atoms of the support are not the critical factors in the present work, although we cannot fully rule out the possibility that the support may be able to change the electronic structure of the catalytic sites. Therefore, we conclude that the key role of the support in photocatalytic water oxidation reaction is to physically separate and immobilize the Co_3O_4 nanoclusters.

Table 5. Photocatalytic Oxygen Evolution Results for Nanoparticle Supports

catalyst	cobalt content (wt %)	O_2 yield (μmol·h^{-1})	TOF (s^{-1} per Co atom) × 10^4
nano-SiO_2/Co_3O_4	4.0	66.8 ± 1.6	3.30 ± 0.08
nano-Al_2O_3/Co_3O_4	4.0	84.3 ± 3.1	4.61 ± 0.17
Co_3O_4 nanoparticles	4.0	46.6 ± 1.2	2.48 ± 0.06

ASSOCIATED CONTENT

Supporting Information

FTIR and UV–vis spectra for mesoporous silica supported cobalt oxide catalysts, TOF calculation, and details for control experiments. This information is available free of charge via the Internet at http://pubs.acs.org/.

AUTHOR INFORMATION

Corresponding Author

*E-mail: jiao@udel.edu.

Notes

The authors declare no competing financial interest.

ACKNOWLEDGMENTS

The authors acknowledge Gregory Hutchings for TEM analysis during the course of the investigation. This work is supported by the University of Delaware Startup Fund.

REFERENCES

(1) Lewis, N. S.; Nocera, D. G. *Proc. Natl. Acad. Sci. U.S.A.* **2006**, *103*, 15729.
(2) Kamat, P. V. *J. Phys. Chem. C* **2007**, *111*, 2834.
(3) Hammarstrom, L.; Winkler, J. R.; Gray, H. B.; Styring, S. *Science* **2011**, *333*, 288.
(4) Gratzel, M. *Nature* **2001**, *414*, 338.
(5) Hurst, J. K. *Science* **2010**, *328*, 315.

(6) Scholes, G. D.; Fleming, G. R.; Olaya-Castro, A.; van Grondelle, R. *Nature Chem.* **2011**, *3*, 763.
(7) Dahl, S.; Chorkendorff, I. *Nat. Mater.* **2012**, *11*, 100.
(8) Asahi, R.; Morikawa, T.; Ohwaki, T.; Aoki, K.; Taga, Y. *Science* **2001**, *293*, 269.
(9) Zou, Z. G.; Ye, J. H.; Sayama, K.; Arakawa, H. *Nature* **2001**, *414*, 625.
(10) Khan, S. U. M.; Al-Shahry, M.; Ingler, W. B. *Science* **2002**, *297*, 2243.
(11) Maeda, K.; Teramura, K.; Lu, D. L.; Takata, T.; Saito, N.; Inoue, Y.; Domen, K. *Nature* **2006**, *440*, 295.
(12) Wang, C.; Xie, Z. G.; deKrafft, K. E.; Lin, W. L. *J. Am. Chem. Soc.* **2011**, *133*, 13445.
(13) Matsumoto, Y.; Sato, E. *Electrochim. Acta* **1979**, *24*, 421.
(14) Okuno, Y.; Yonemitsu, O.; Chiba, Y. *Chem. Lett.* **1983**, 815.
(15) Harriman, A.; Pickering, I. J.; Thomas, J. M.; Christensen, P. A. *J. Chem. Soc. Faraday Trans. I* **1988**, *84*, 2795.
(16) Hara, M.; Waraksa, C. C.; Lean, J. T.; Lewis, B. A.; Mallouk, T. E. *J. Phys. Chem. A* **2000**, *104*, 5275.
(17) Brimblecombe, R.; Swiegers, G. F.; Dismukes, G. C.; Spiccia, L. *Angew. Chem., Int. Ed.* **2008**, *47*, 7335.
(18) Kanan, M. W.; Nocera, D. G. *Science* **2008**, *321*, 1072.
(19) Esswein, A. J.; McMurdo, M. J.; Ross, P. N.; Bell, A. T.; Tilley, T. D. *J. Phys. Chem. C* **2009**, *113*, 15068.
(20) Kohl, S. W.; Weiner, L.; Schwartsburd, L.; Konstantinovski, L.; Shimon, L. J. W.; Ben-David, Y.; Iron, M. A.; Milstein, D. *Science* **2009**, *324*, 74.
(21) Lutterman, D. A.; Surendranath, Y.; Nocera, D. G. *J. Am. Chem. Soc.* **2009**, *131*, 3838.
(22) Risch, M.; Khare, V.; Zaharieva, I.; Gerencser, L.; Chernev, P.; Dau, H. *J. Am. Chem. Soc.* **2009**, *131*, 6936.
(23) Brimblecombe, R.; Koo, A.; Dismukes, G. C.; Swiegers, G. F.; Spiccia, L. *J. Am. Chem. Soc.* **2010**, *132*, 2892.
(24) Jiao, F.; Frei, H. *Energy Environ. Sci.* **2010**, *3*, 1018.
(25) Jiao, F.; Frei, H. *Chem. Commun.* **2010**, *46*, 2920.
(26) Najafpour, M. M.; Ehrenberg, T.; Wiechen, M.; Kurz, P. *Angew. Chem., Int. Ed.* **2010**, *49*, 2233.
(27) Robinson, D. M.; Go, Y. B.; Greenblatt, M.; Dismukes, G. C. *J. Am. Chem. Soc.* **2010**, *132*, 11467.
(28) Boppana, V. B. R.; Jiao, F. *Chem. Commun.* **2011**, *47*, 8973.
(29) Najafpour, M. M. *Dalton Trans.* **2011**, *40*, 3805.
(30) Shevchenko, D.; Anderlund, M. F.; Thapper, A.; Styring, S. *Energy Environ. Sci.* **2011**, *4*, 1284.
(31) Wang, D. E.; Li, R. G.; Zhu, J.; Shi, J. Y.; Han, J. F.; Zong, X.; Li, C. *J. Phys. Chem. C* **2012**, *116*, 5082.
(32) Man, I. C.; Su, H. Y.; Calle-Vallejo, F.; Hansen, H. A.; Martinez, J. I.; Inoglu, N. G.; Kitchin, J.; Jaramillo, T. F.; Norskov, J. K.; Rossmeisl, J. *ChemCatChem* **2011**, *3*, 1159.
(33) McCool, N. S.; Robinson, D. M.; Sheats, J. E.; Dismukes, G. C. *J. Am. Chem. Soc.* **2011**, *133*, 11446.
(34) Cong, Y. Q.; Park, H. S.; Dang, H. X.; Fan, F. R. F.; Bard, A. J.; Mullins, C. B. *Chem. Mater.* **2012**, *24*, 579.
(35) Gao, M. R.; Xu, Y. F.; Jiang, J.; Zheng, Y. R.; Yu, S. H. *J. Am. Chem. Soc.* **2012**, *134*, 2930.
(36) Hong, D.; Jung, J.; Park, J.; Yamada, Y.; Suenobu, T.; Lee, Y. M.; Nam, W.; Fukuzumi, S. *Energy Environ. Sci.* **2012**, *5*, 7606.
(37) Iyer, A.; Del-Pilar, J.; King'ondu, C. K.; Kissel, E.; Garces, H. F.; Huang, H.; El-Sawy, A. M.; Dutta, P. K.; Suib, S. L. *J. Phys. Chem. C* **2012**, *116*, 6474.
(38) Ma, S. S. K.; Maeda, K.; Abe, R.; Domen, K. *Energy Environ. Sci.* **2012**, *5*, 8390.
(39) Moonshiram, D.; Jurss, J. W.; Concepcion, J. J.; Zakharova, T.; Alperovich, I.; Meyer, T. J.; Pushkar, Y. *J. Am. Chem. Soc.* **2012**, *134*, 4625.
(40) Sartorel, A.; Carraro, M.; Toma, F. M.; Prato, M.; Bonchio, M. *Energy Environ. Sci.* **2012**, *5*, 5592.
(41) Tran, P. D.; Wong, L. H.; Barber, J.; Loo, J. S. C. *Energy Environ. Sci.* **2012**, *5*, 5902.
(42) McAlpin, J. G.; Stich, T. A.; Ohlin, C. A.; Surendranath, Y.; Nocera, D. G.; Casey, W. H.; Britt, R. D. *J. Am. Chem. Soc.* **2011**, *133*, 15444.
(43) Young, E. R.; Costi, R.; Paydavosi, S.; Nocera, D. G.; Bulovic, V. *Energy Environ. Sci.* **2011**, *4*, 2058.
(44) Surendranath, Y.; Lutterman, D. A.; Liu, Y.; Nocera, D. G. *J. Am. Chem. Soc.* **2012**, *134*, 6326.
(45) Jiao, F.; Frei, H. *Angew. Chem., Int. Ed.* **2009**, *48*, 1841.
(46) Kleitz, F.; Choi, S. H.; Ryoo, R. *Chem. Commun.* **2003**, 2136.
(47) Zhao, D. Y.; Feng, J. L.; Huo, Q. S.; Melosh, N.; Fredrickson, G. H.; Chmelka, B. F.; Stucky, G. D. *Science* **1998**, *279*, 548.
(48) Jiao, F.; Bruce, P. G. *Adv. Mater.* **2007**, *19*, 657.
(49) Yen, H.; Seo, Y.; Guillet-Nicolas, R.; Kaliaguine, S.; Kleitz, F. *Chem. Commun.* **2011**, *47*, 10473.
(50) van der Meer, J.; Bardez, I.; Bart, F.; Albouy, P. A.; Wallez, G.; Davidson, A. *Microporous Mesoporous Mater.* **2009**, *118*, 183.
(51) Jiu, J. T.; Ge, Y.; Li, X. N.; Nie, L. *Mater. Lett.* **2002**, *54*, 260.
(52) Mekhemer, G. A. H.; Abd-Allah, H. M. M.; Mansour, S. A. A. *Colloids Surf. Phys. Eng. Aspects* **1999**, *160*, 251.
(53) Gardner, G. P.; Go, Y. B.; Robinson, D. M.; Smith, P. F.; Hadermann, J.; Abakumov, A.; Greenblatt, M.; Dismukes, G. C. *Angew. Chem., Int. Ed.* **2012**, *51*, 1616.
(54) Yamada, Y.; Yano, K.; Hong, D. C.; Fukuzumi, S. *Phys. Chem. Chem. Phys.* **2012**, *14*, 5753.